ACS OMEGA

http://pubs.acs.org/journal/acsodf

Article

A Multiwalled Carbon Nanotube-Based Polyurethane Nanocomposite-Coated Sand/Proppant for Improved Mechanical Strength and Flowback Control in Hydraulic Fracturing Applications

Ali Aref Ali Alzanam, Umair Ishtiaq, Ali Samer Muhsan,* and Norani Muti Mohamed

Cite This: *ACS Omega* 2021, 6, 20768−20778

Read Online

ACCESS | Metrics & More | Article Recommendations

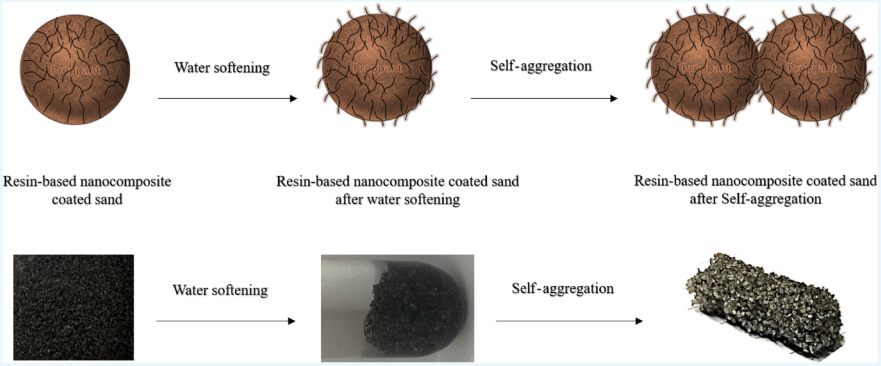

ABSTRACT: A novel resin-based nanocomposite-coated sand proppant is introduced to address the issue of proppant flowback in post-fracturing fluid flowback treatments and hydrocarbon production. Self-aggregation in the water environment is the most attractive aspect of these developed proppants. In this work, sand was sieve-coated with 0.1% multiwalled carbon nanotubes (MWCNTs) followed by optimized thin and uniform resin (polyurethane) spray coating in the concentration range of 2 to 10%. Quantitative and qualitative evaluations have been carried out to assess the self-aggregation capabilities of the proposed sand proppants where no flowback was witnessed at 4% polyurethane coating containing 0.1% MWCNTs. This applied resin incorporating MWCNT coating was characterized by field emission scanning electron microscopy, and energy-dispersive X-ray spectroscopy depicted the dispersed presence of MWCNTs into polyurethane resin corroborated by the presence of 38% elemental carbon on the sand substrate. Proppant crushing resistance tests were conducted, including proppant pack stress−strain response, compaction, and fines production. It was found that the proposed sand proppant decreased the proppant pack compaction by ∼25% compared to commonly used silica sand with the ability to withstand high closure stress as high as 55 MPa with less than 10 wt % fines production. The surface wettability was determined by the sessile drop method. The application of resin incorporating MWCNT coating layers changed the sand proppant wetting behavior to oil-wet with a contact angle of ∼124°. Thermogravimetric analyses revealed a significant increment in thermal stability, which reached up to 280 °C due to the addition of MWCNTs as reinforcing nanofillers.

1. INTRODUCTION

Hydraulic fracturing, also commonly referred to as "fracking", is a famously employed well stimulation technique that involves fracturing shale-rock formations by injecting a pressurized fluid.[1,2] In this process, a synthesized fracking fluid is pumped into the wellbore at high pressures to propagate cracks (fractures) in the deep rock formations creating interconnected fracture channel pathways as passages for the entrapped hydrocarbon to flow out into the production tubing.[3−9] The fracking fluid comprises various components such as water, proppant particles, polymers, chemicals, etc.[7,10] When the hydraulic pressure is removed from the well, the injected proppant grains' main purpose is to hold the fractures open for hydrocarbon production.[11−15]

Proppants are a solid material, typically sand, treated sand, or a manufactured ceramic-based material, designed to be injected to prevent and maintain an induced hydraulic fracture open during and after a fracturing treatment so that the

Received: March 26, 2021
Accepted: June 23, 2021
Published: August 5, 2021

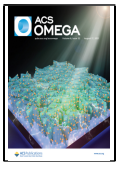

https://doi.org/10.1021/acsomega.1c01639
ACS Omega 2021, 6, 20768−20778

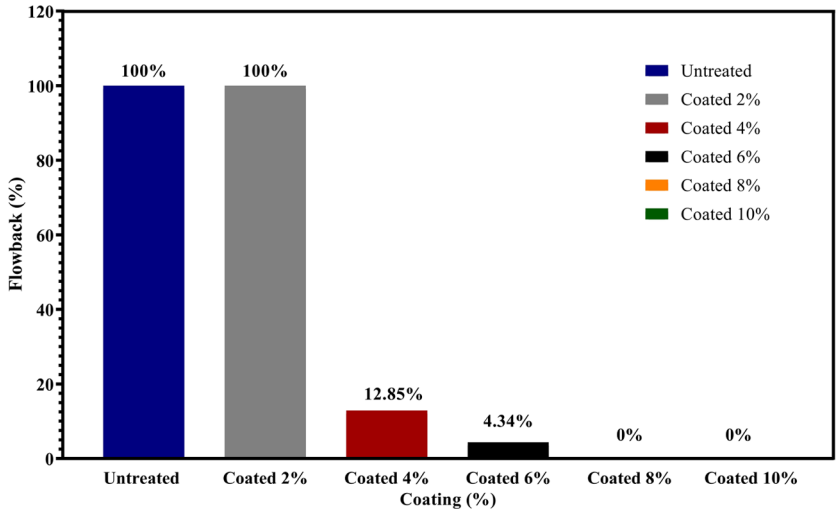

Figure 1. Quantitative evaluation of sand self-aggregation (flowback control) at different polyurethane resin concentrations.

fracture does not collapse and close.[16] For further visualization, refer to ref 17. Raw silica sand is one of the most commonly used proppant materials, accounting for more than 96.4% of the proppant market in 2016.[18] The proppant's primary purpose is to keep the hydraulically induced fractures open and conductive by acting as a mechanically robust support particle that provides a conductive pathway for hydrocarbons to flow from the reservoir to the wellbore.[19] Thus, the stimulation effect of hydraulic fracturing is dictated explicitly by the proppant's performance and placement pattern.[17]

The most prevalent issue following hydraulic fracturing treatment is proppant flowback.[1] Proppant flowback can be caused by several factors, including high drag forces of a flowing fluid at a high velocity, low fracture closure stress, mechanical properties of the treated formation, high viscosity of the produced fluid, and inappropriate proppant size or density.[20] Proppant flowback has various negative implications, including narrowing the fracture's diameter, lowering the fracture's conductivity, and decreasing the treatment's effectiveness.[21] Furthermore, proppants discharged into the well will erode downhole equipment and surface pipelines and equipment, reducing their service lifetime.[22]

In hydraulic fracking, controlling proppant flowback has always been an issue. In the 1980s, Pope et al. introduced the curable resin-coated proppant (RCP) to the oil industry for the first time.[23] Peard et al.[24] and Terracina et al.[25] had used various types of resins to coat the proppants, including epoxy resin, phenolic resin, furfural resin, and furfuralcohol resin. They pointed out that choosing a suitable resin for different conditions will prepare a successful RCP to prevent proppant flowback. In comparison, an RCP's cured proppant pack provides chemical bonding between grains to prevent proppant flowback. An RCP is typically only partially cured during storage and transportation, resulting in the RCP's inability to provide adequate consolidation strength to the proppant pack and a weaker proppant flowback control capability.[26] Furthermore, the partially cured coated proppant generally requires the addition of chemical activators and a particular temperature to cure,[27] increasing the cost of the coating process. Another efficient approach for controlling proppant flowback is to inject fibers into the fracturing fluid with the proppants.[28] Unlike resin-coated proppants, fibers provide a framework and only use the physical bonding effect to hold them together. As a result, the permeability of the proppant pack is unaffected. On the other hand, fibers are easily broken into smaller fragments, causing injection blockage.[29,30] If the proppants are out of their original places, then both resin-coated proppants and fiber-bound proppants are ineffective.

Another common issue is fines generation caused by an overly stressed proppant, which either reduces the flow current or completely blocks the fracture.[16,31] Thus, polymers and/or resins were introduced to the sand proppants to allow them to withstand such high downhole closure stresses, thereby improving flow conductivity.[32,33] The primary benefit of using coated sand as a proppant is that the coating effectively traps the broken grains inside the matrix. For further visualization, refer to ref 34. Moreover, proppants should be further improved with mechanically reinforced polymer composites to improve the efficiency of traditional RCPs in the downhole to withstand high closure stresses.[18]

Epoxy resin is the most widely used polymer for proppant coating due to its high mechanical strength and capability to prevent proppant flowback. However, at high temperatures, the epoxy matrix is weakened and aggregated, affecting the fractures' flow current.[35] Incorporating nanofillers like graphene and carbon nanotubes into the coating layer will potentially solve this problem.[36] With their appreciable nanomechanical properties, reinforced polymer composites may be a possible candidate to improve the stress resistance of the coated sand proppants even further and provide high thermal stability.

This work introduces and evaluates a thin resin-based nanocomposite (polyurethane reinforced with multiwalled carbon nanotubes (MWCNTs))-coated sand to prevent the proppant flowback incident as well as to enhance the sand proppant mechanical and thermal properties. The proposed proppants could aggregate in liquid conditions and reaggregate when the proppants are dispersed into streaming sands. The proposed proppant self-aggregation property was studied. Further investigations, including sand proppant coating characterization and contact angle measurement, were conducted. All tests except for TGA were performed at ambient conditions.

https://doi.org/10.1021/acsomega.1c01639
ACS Omega 2021, 6, 20768−20778

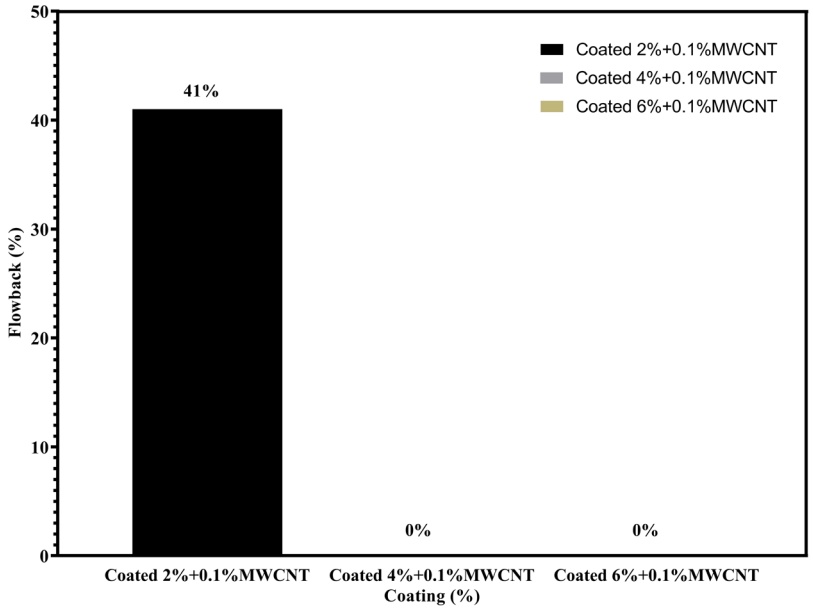

Figure 2. Quantitative evaluation of resin-based nanocomposite-coated sand self-aggregation (flowback control) at different polyurethane resin concentrations.

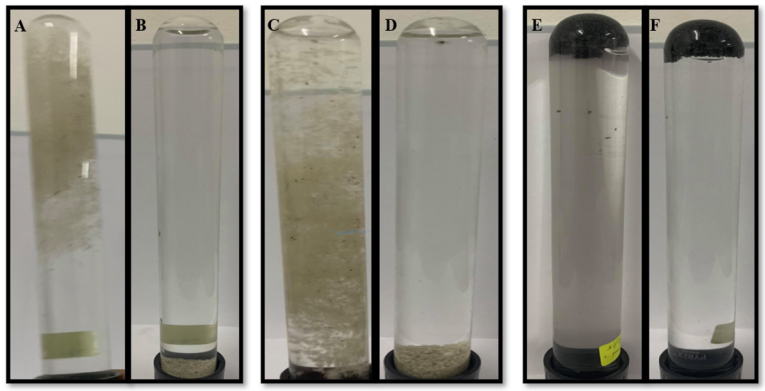

Figure 3. Pictures of aggregation states of (A,B) untreated sand, (C,D) resin-coated sand, and (E,F) resin-based nanocomposite-coated sand.

2. RESULTS AND DISCUSSION

2.1. Proppant Self-Aggregation Measurement. The statistical result of sand self-aggregation characteristics (flowback control) is shown in Figure 1. The untreated sand proppant with no coating applied shows complete sand flowback that clearly manifests the absence of any adhesive bonding among the sand grains. Likewise, even 2% polyurethane coating concentration fails to create adequate adhesive bonding that can provide resistance to flowback. However, doubling the polyurethane concentration to 4% significantly reduces the sand flowback to around 87%. An adequate amount of coating is now available on the surface that creates sufficient mutual adhesion among the coated sand grains to resist the flowback force effectively. A further step-up in the coating concentration to 6% reduces sand flowback to about 95% followed by no flowback at 8 and 10%.

To enhance closure stress resistance, thermal stability, and adhesive (bonding) potential of polyurethane resin coating, a resin-based nanocomposite was prepared by incorporating MWCNTs into the polymer matrix of polyurethane coating. As shown in Figure 2, the addition of 0.1% MWCNTs into 2% polyurethane coating significantly improved flowback to around 60%, whereas when compared to that without MWCNTs, all the mass conveniently flowed back due to the absence of any bonding within the proppant pack as depicted in Figure 1. However, keeping the MWCNT amount constant at 0.1% but increasing the polyurethane coating concentration to 4% revealed no flowback, as shown in Figure 2. This was due to the fact that dual adhesive forces with enhanced polyurethane polymeric strength were in play in the polyurethane-MWCNT hybrid coating. The polymeric covalent bonding potential of the polyurethane polymer matrix was significantly augmented by MWCNT fillers that acted as molecular anchors as well as supplementary cross-linking agents for polyurethane polymer chains.[37,36]

2.2. Proppant Self-Aggregation Characteristics. The self-aggregation property of the resin-based nanocomposite-coated sand was tested qualitatively by its status in a sample bottle filled with brine solution mimicking the fracturing fluid when the bottle was turned upside down. As shown in Figure 3A,B, the untreated sands still scattered particles and instantly

https://doi.org/10.1021/acsomega.1c01639
ACS Omega 2021, 6, 20768−20778

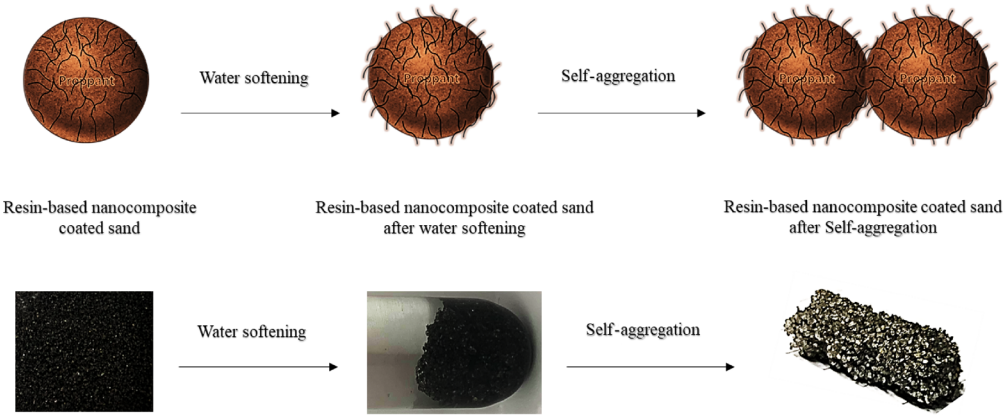

Figure 4. Diagram depicting the resin-based nanocomposite-coated sand self-aggregation process.

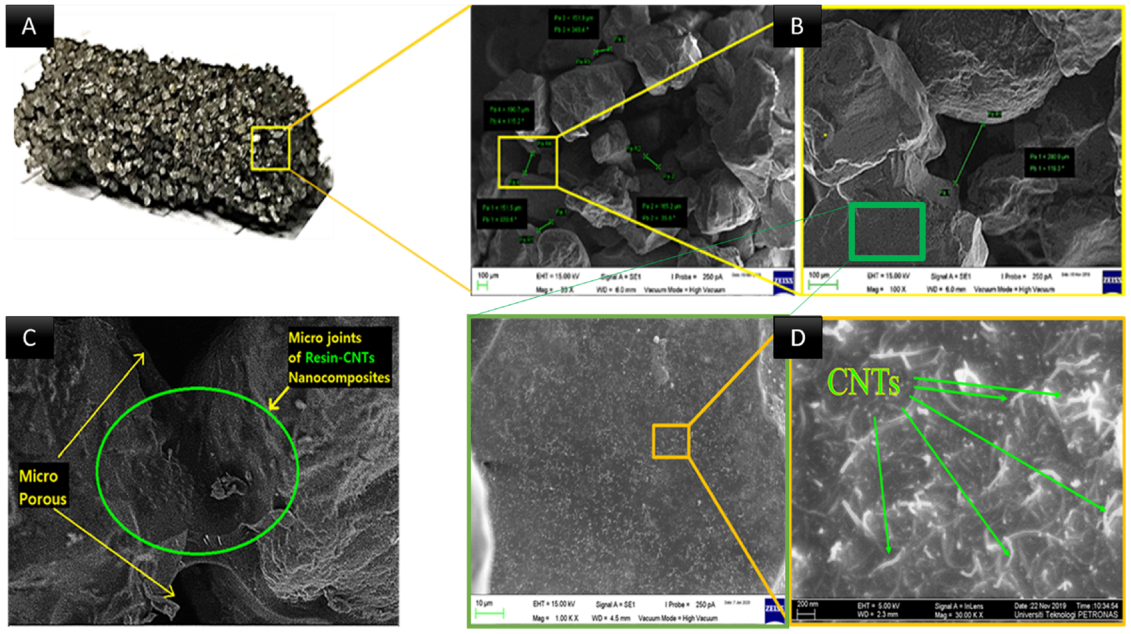

Figure 5. (A) Self-aggregated resin-based nanocomposite-coated sand pack. (B) FESEM micrographs showing the porous well-joint structure of the pack. (C) FESEM micrograph displaying the formation of resin microjoints. (D) FESEM micrographs presenting highly dispersed MWCNTs on the sand surface.

dropped them to the bottom; the same observations were noticed with resin-coated sand (coated with 4 wt % polyurethane resin), as presented in Figure 3C,D. However, when it comes to the resin-based nanocomposite-coated sand (coated with 0.1 wt % MWCNTs followed by 4 wt % polyurethane resin), sand grain conglomeration was created and stuck on the top of the bottle as a consolidated proppant pack, as revealed in Figure 3E,F.

Based on this qualitative evaluation, it is fair to suggest that the proposed resin-based nanocomposite-coated sand exhibited a self-aggregation property in brine. The mechanism behind this aggregation property is that when the proposed proppants (the resin-based nanocomposite-coated sand) were applied to brine, the dry coating transformed into flexible long-chain groups due to the water softening effect. The flexible long-chain groups interacted and created a complete structure among the grains, resulting in sand congeries, as illustrated in Figure 4.

2.3. Characterization of Sand Coating. It was previously deduced that the adhesive potential of polyurethane resin coating was significantly enhanced by the inclusion of MWCNTs into the polymer coating. To corroborate this finding, microscopy images of the resin-based nanocomposite-coated sand particles are shown in Figure 5 at different magnifications using a field emission scanning electron microscope (FESEM; model, Zeiss Supra 55 VP; manufacturer, ZEISS). An energy-dispersive X-ray analyzer determined the carbon element presence representing MWCNTs on the coated sand grains (EDX), refer to Table 1. The result confirms the existence of carbon on the sand proppant by 38%.

Table 1. EDX Elemental Analysis

element	weight %
C	38.33
O	35.99
Al	0.63
Si	24.53
Cl	0.52

https://doi.org/10.1021/acsomega.1c01639
ACS Omega 2021, 6, 20768−20778

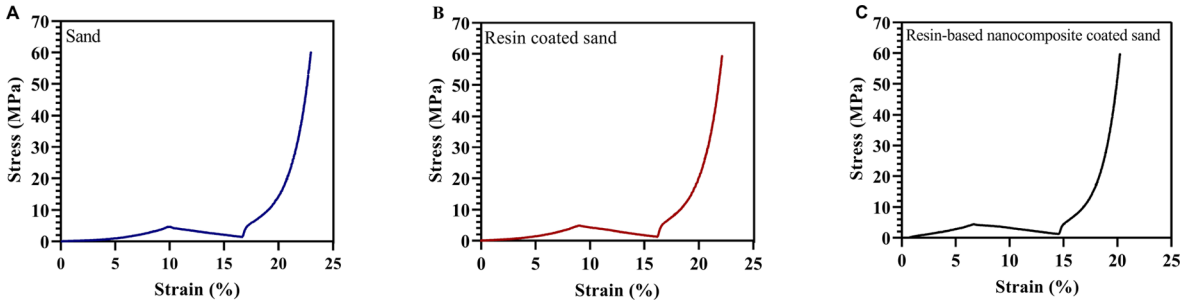

Figure 6. Stress–strain response of (A) sand, (B) resin-coated sand, and (C) resin-based nanocomposite-coated sand.

A coalesced sand pack having a mild blackish color texture visibly confirms the presence of MWCNTs, as shown in Figure 5A. Without any coating, these sand particles were in a loose granular form. It appears that the fast cured polyurethane incorporating MWCNT resin coating forms a porous well-joint structure, as shown in Figure 5B. The presence of these well-connected joints reduces interparticle pore size but on the contrary renders good resistance against proppant flowback under the influence of any driving forces.

One important observation to make is that it seems discernable that the sand particles are physically well-joint together. However, as shown in Figure 5C, the polymer resin forms a linkage between the sand particles without them being in actual physical contact. This polyurethane resin system creates microconnecting bridges among the sand particles, thus making them immobile. This microbridging of proppants offers an advantage to allow permeation of reservoir fluids and not make the proppant pack fully dense. As shown in Figure 5D, the presence of dispersed MWCNTs with minor traces of flocculation acts as a reinforcement additive fiber, keeping the sand particles well-connected and thus allowing for high proppant flowback control.

The high degree of cross-linking tends to be present in polyurethane coatings, manifesting a three-dimensional (3D) cross-linked network.[38] The inclusion of MWCNTs into this polyurethane coating forms an additional interconnected CNT fiber network structure that well interweaves with the polyurethane polymer chain structure. These interwoven cross-linked polyurethane polymer chains with CNT fibers greatly enhance the mutual proppant particle bonding ability via microbridging, as shown in Figure 5C, which almost eliminates proppant flowback.

2.4. Behavior of Proppant Packs under a Subjected Load. Three different proppants (sand, resin-coated sand, and resin-based nanocomposite-coated sand) were specifically investigated based on stress–strain response to consider proppant pack behavior when exposed to loading conditions. Figure 6A–C presents the stress versus strain deviation of each type of proppant. Each type of proppant was positioned on the crushing cell and subsequently subjected to a maximum peak stress of 55 MPa.

As shown in Figure 6, all three proppants have provided almost similar mechanical responses showing a slow increase in stress during the loading cycle. It is critical to understand how these proppant packs respond under various stress conditions. According to Omidvar et al.,[39] three major mechanisms lead to uniaxial sand compression: (1) elastic compression of individual grains, (2) grain slippage and rearrangement, and (3) grain crushing. Based on their governing mechanism, the authors described four distinct stages in granular response to uniaxial compression. When comparing Omidvar et al.'s granular response to the three proppant forms, it becomes clear that each proppant pack exhibits substantial strain hardening (locking-up) behavior at the start of the load cycle. Significant rearrangement of proppants into voids is predicted during this hardening (locking-up) process, resulting in a denser pack arrangement, increasing the grain–grain contacts, and decreasing the grain's ability to slip and move.

Additionally, proppant crushing occurs at higher stress levels in conjunction with the proppant hardening process, facilitating proppant pack compression even more. In the subsequent sections, the degree of proppant crushing demonstrated by various proppant types is detailed. To quantify the proppants' stress–strain response, the constrained modulus was computed at stresses between 5 and 50 MPa as in eq 1, and the results are shown in Figure 7.

$$\text{Constrained modulus} = \frac{\text{Change in stress between 5 and 50 MPa}}{\text{Change in strain at 5 and 50 MPa}} = \frac{\Delta\sigma}{\Delta\varepsilon} \quad (1)$$

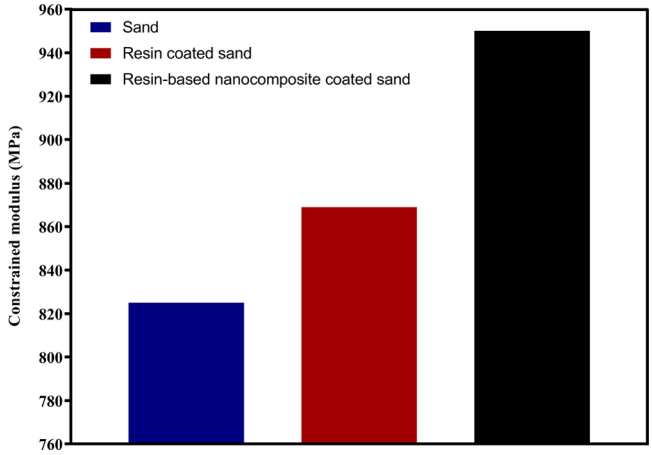

Figure 7. Constrained modulus calculation results for sand, resin-coated sand, and resin-based nanocomposite-coated sand.

The resin-based nanocomposite-coated proppant recorded the highest constrained modulus with 950 MPa compared to uncoated sand and resin-coated sand with 825 and 869 MPa, respectively, as shown in Figure 7. The constrained modulus is inversely proportional to pack compressibility. Thus, the proposed resin-based nanocomposite-coated proppant less-

https://doi.org/10.1021/acsomega.1c01639
ACS Omega 2021, 6, 20768–20778

ened the compressibility of the proppant pack by 13.1% as compared to untreated silica sand.

Another set of calculations was conducted to measure the variation of proppant pack compaction as they are subjected to 55 MPa. The proppant pack compaction was determined using eq 2.

$$\text{Proppant pack compaction (\%)} = \frac{\text{Deformation of the proppant pack}}{\text{Original height of the proppant pack}} \times 100 \quad (2)$$

Figure 8 presents the proppant pack compaction results. All forms of proppants showed a substantial increase in proppant

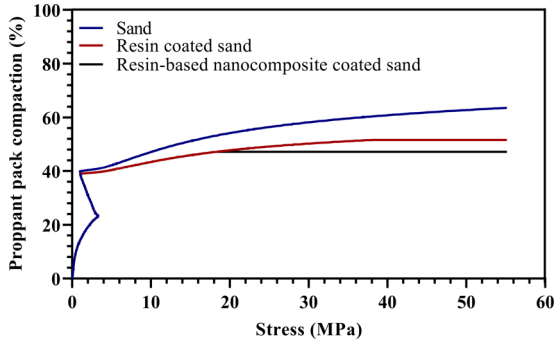

Figure 8. Proppant pack compaction measurement for sand, resin-coated sand, and resin-based nanocomposite-coated sand.

pack compaction, as shown in Figure 8. This implies that, regardless of the proppant type, all proppants appear to undergo substantial proppant pack compaction and porosity reduction due to the strong in situ confining stresses that occur underground. However, based on the result displayed in Figure 8, proppant pack compaction was decreased by 63.6, 51.7, and 47.2% for sand, resin-coated sand, and resin-based nanocomposite-coated sand, respectively. The extreme compaction that occurred inside the sand and resin-coated proppants would significantly reduce the porosity of the proppant pack. This behavior may be due to a large amount of particle crushing and the production of fines, which allows proppants to be rearranged within voids.

2.5. Proppant Fines Production Measurement. Based on the API standard, proppants can be considered as high-strength if it generates fines less than 10% after a crushing test.[40] Fines are described as loose and unconsolidated particles that are typically smaller than 37 μm.[41,42] In this work, stress levels of 27.6 and 55.2 MPa were applied on untreated sand, resin (polyurethane)-coated sand, and resin-based nanocomposite-coated sand. As shown in Figure 9, high amounts of fines, i.e., 15.63 and 22.58%, were generated by untreated sand at different stress levels, which are extremely above the threshold limit of 10%. By coating the sand with polyurethane resin, fines generated under the applied stresses were within the prescribed limit. Noticeable reduction in fines generation was attributed to the protective encapsulation of polyurethane resin coating that contained the fines generated within the proppant body.[34,43] The applied polymeric layer provides grain-to-grain bonding that evenly distributes the applied load stress within the proppant mass. Doubling the stress level to 55.2 MPa has increased fines generation by 2%, which indicates an effective load distribution and fines containment within the polyurethane coating. For resin-based nanocomposite-coated sand, fines generated at 27.6 MPa were 6.25%, slightly lesser than those of polyurethane-coated sand. At this initial loading, a considerable percentage of fines generation can be associated with proppant reorientation (pack adjustment) and not fully developed grain-to-grain bonding. Interestingly, when the stress load was doubled to 55.2 MPa, there was only a 0.20% increment in the generated fines. This indicates a high-strength structural covering by a hybrid coating of a polyurethane cross-linked structure incorporated with an MWCNT network. It was also deduced that this remarkable reduction in fines generation at 55.2 MPa (6.27%) was mainly due to the high modulus of elasticity and large specific surface area of MWCNTs, which physically interact with the resin matrix creating a dense three-dimensional cross-linked polyurethane-MWCNT hybrid coating that facilitates a higher distribution of the applied stress load and efficient containment of the generated fines.[44]

2.6. Contact Angle Measurement. To determine the wettability alteration potential of resin-coated sand grains from hydrophilic to hydrophobic, the contact angle was measured by utilizing the sessile drop method (Figure 10). Three samples were prepared in molds, as shown in Figure 11. Each drop of 2% KCl solution that mimics the formation water was placed on the prepared sand samples. As shown in Figure 10A, untreated sand was completely hydrophilic (water-wet). In Figure 10B, the contact angle (θ) of polyurethane-coated sand came out to be 111° that clearly indicated a shift to

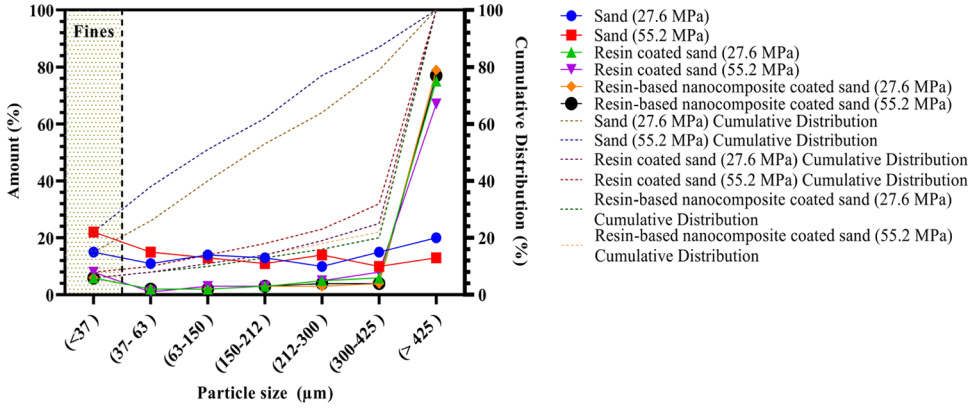

Figure 9. Particle size distribution vs the amount and cumulative distribution of sand, resin-coated sand, and resin-based nanocomposite-coated sand at different stress levels.

https://doi.org/10.1021/acsomega.1c01639
ACS Omega 2021, 6, 20768−20778

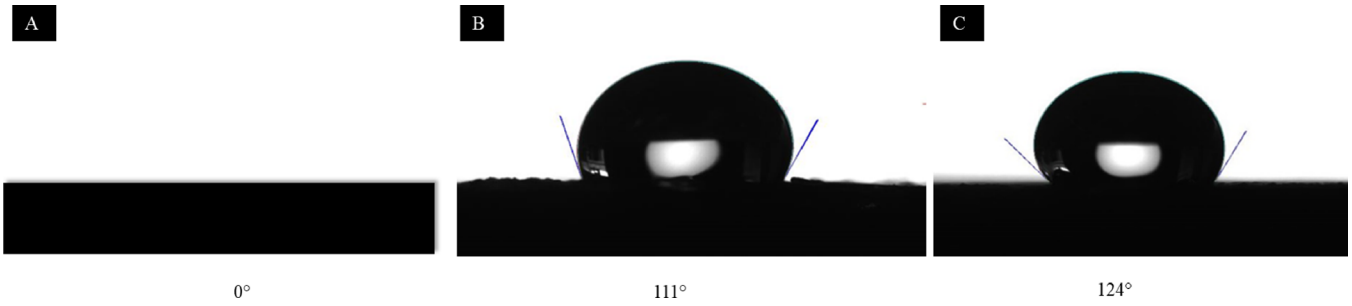

Figure 10. Contact angle measurement of (A) untreated sand, (B) resin-coated sand, and (C) resin-based nanocomposite-coated sand.

Figure 11. Water droplet on (A) sand pack, (B) resin-coated sand pack, and (C) resin-based nanocomposite-coated pack.

hydrophobic tendency due to the application of polyurethane coating on the sand particles. Polyurethanes have a hydrophobic wetting behavior in nature.[45] This hydrophobic tendency was further augmented by the increment in the contact angle (θ) to 124° for the resin-based nanocomposite-coated sand proppant, as shown in Figure 10C. The presence of MWCNTs increases the coating layer's surface roughness, which explains the slight modification in contact angle. The surface wettability of uncoated sand from hydrophilic was clearly altered to hydrophobic by the application of polyurethane incorporating MWCNT coating on the sand. This removes virtually the capillary forces, which prevent the water and fracturing fluids from being trapped after and during fracturing,[46] hence leading to potential proppant scale prevention and better hydrocarbon flow.

2.7. TGA Test for Proppant Thermal Stability. The thermal properties of different coating layers have been measured via TGA. The initial decomposition temperature is the temperature at which your material begins to disintegrate, and it is a measure of the material's thermal stability. Figure 12 presents the TGA curves of resin-coated sand (coated with 4 wt % polyurethane resin) and resin-based nanocomposite-coated sand (coated with 0.1 wt % MWCNTs followed by 4 wt % polyurethane resin). The degradation temperature point (T_{deg}) for both types of coated sands was recorded. The T_{deg} of the resin-coated sand was 113 °C, as shown by the TGA curves, which is typical for polyurethane as its thermal stability ranges from 90 to 120 °C.[16] Incorporating MWCNTs on the coating layer significantly increased the T_{deg} to 280 °C. This is due to the fact that MWCNT decomposition occurs at a higher temperature that can reach more than 400 °C.[47] The substantial improvement of thermal conductance is remarkable for the resin-based nanocomposite-coated sand. The presence of MWCNTs acts like a bridge that holds the resin matrix providing additional thermal stability.[36]

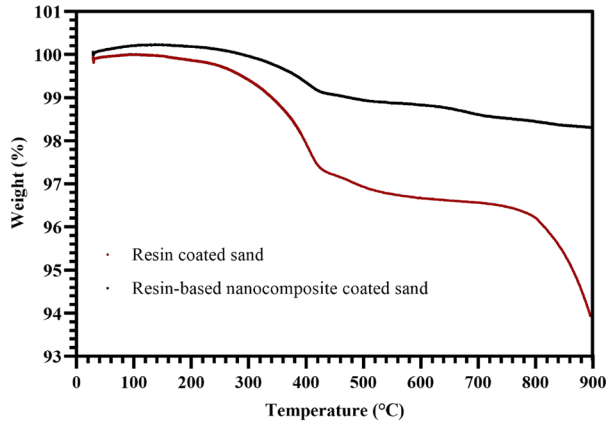

Figure 12. TGA curves for resin-coated sand and resin-based nanocomposite-coated sand.

3. CONCLUSIONS

After hydraulic fracturing treatment, proppant flowback is an unavoidable problem. A novel resin-based nanocomposite-coated sand was introduced to create mutual adhesion by creating grain-to-grain bonding to prevent proppant flowback. The resin-based nanocomposite-coated sand proppants' distinctive self-aggregating property in the liquid environment is explained by the water softening effect. An assessment method based on the air driving force effect was developed as a new idea for proppant flowback control. Also, it is used to measure the aggregating strength of the proppant pack, which introduces the optimal surface coating formula of 0.1 wt % multiwalled carbon nanotube (MWCNT) incorporation 4 wt % polyurethane resin (resin-based nanocomposite). Further laboratory testing was conducted to test the proposed coating layer's ability to enhance mechanical strength, alter the wetting behavior, and increase thermal stability. According to the findings of the investigations mentioned above, the following conclusions can be drawn:

- Resin-based nanocomposite coating layers provide sufficient bonding strength that prevents sand/proppant flowback.
- The proposed sand proppant reduced proppant pack compaction by 25% compared to widely used silica sand and could resist high closure stress as high as 55 MPa with less than 10% fines.
- Wettability measurement suggested that resin-based nanocomposite coating layers were able to change the

https://doi.org/10.1021/acsomega.1c01639
ACS Omega 2021, 6, 20768−20778

proppant wetting behavior to oil-wet with a contact angle of ∼124°.
- The thermal stability of the proposed sand proppant reached up to 280 °C.

Future researchers are recommended to assess the proposed proppants' capability to control flowback at reservoir conditions. It is also advised to conduct the crushing test at different temperatures while proppants are in contact with the fluid to mimic the reservoir conditions.

4. EXPERIMENTAL STUDY

4.1. Materials. Sand (20/50 mesh) used as a proppant was obtained from Kim Yuan Amang Sdn. Bhd., Malaysia.

Table 2. XRF Results for Sand and Polyurethane

material	sand	polyurethane
SiO_2 (%)	95.0	
CaO (%)	0.324	24.3
P_2O_5 (%)	1.56	4.84
Al_2O_3 (%)	2.74	
K_2O (%)	0.121	
Fe_2O_3 (%)	0.142	0.450
TiO_2 (%)	0.136	
ZrO_2 (%)		59.1
CoO (%)		10.3

Polyurethane was obtained from Weifang Waterproof Materials Co., Ltd. Multiwalled carbon nanotubes (MWCNTs) with a length between 0.5 and 2 μm, an outer diameter between 30 and 50 nm, and a surface area of 60m^2/g were obtained from Sigma Aldrich, Houston, TX, USA. All the materials were used as received. Further analysis of sand and commercial polyurethane shown in Table 2 was performed by X-ray fluorescence (XRF).

4.2. Sample Preparation (Proppant Coating). The sand coating process is composed of two main stages. In the first stage, dry coating was performed in which the sand proppant was sieve-coated by MWCNTs, as shown in Figure 13A. In this context, MWCNTs were positioned on a sieve with a 400 US mesh size followed by sand on the underneath pan. Then, they were vibrated for 5 min using a sieve shaker. The sieve-coating objectives were to reduce agglomeration and promote highly dispersed placement of MWCNTs on the sand proppant

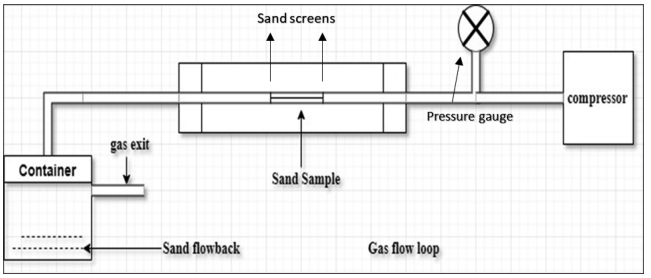

Figure 14. Gas loop system setup.

Table 3. Synthetic Water Composition

composition	NaCl	KCl	$CaCl_2$	$MgCl_2$	TDS[a]
concentration (g/L)	28.0	0.935	1.19	5.368	35.493

[a]TDS, total dissolved solids.

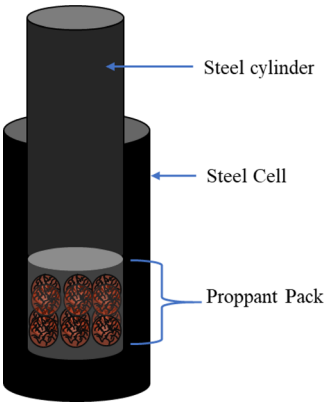

Figure 15. Schematic view of proppant files on the crushing cell.

substrate. The MWCNT nanoparticles would be mounted on the proppant as they move through the sieve. Due to the multiwalled structure of CNTs, the cylindrical walls form forces between the carbon atoms and the sand substrate.[48] Electrostatic forces and surface energy forces, including van der Waals forces, are responsible for cohesion (intermolecular potential energy).

In the second stage, polyurethane resin was sprayed to sand by utilizing a high-velocity spray gun with a spray angle of 30° and a spray distance of 38 cm,[49] as shown in Figure 13B. The

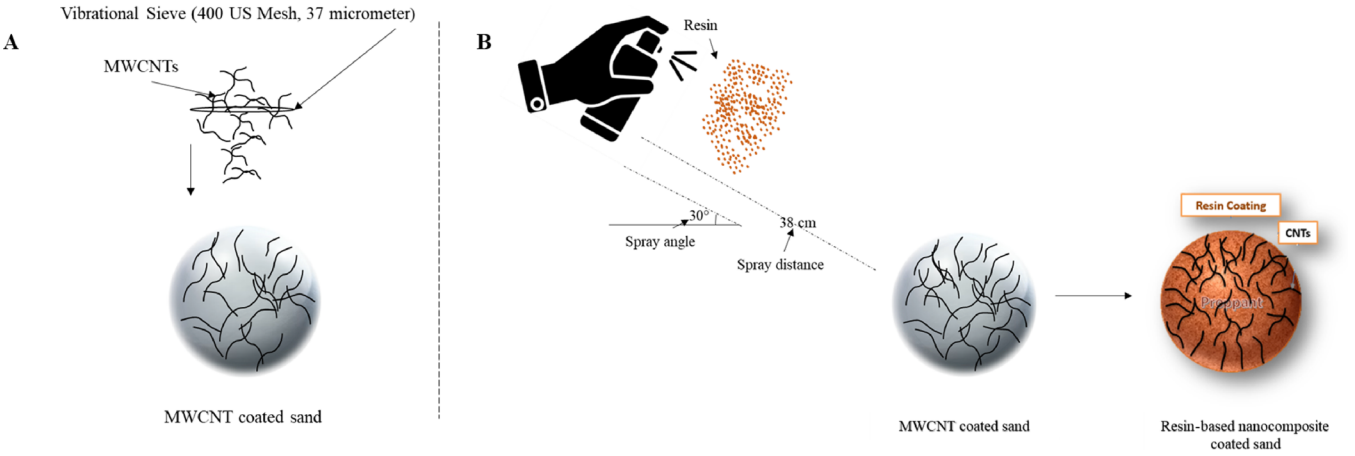

Figure 13. Sand coating process: (A) first stage, MWCNT dry coating and (B) second stage, polyurethane resin spray coating.

https://doi.org/10.1021/acsomega.1c01639
ACS Omega 2021, 6, 20768−20778

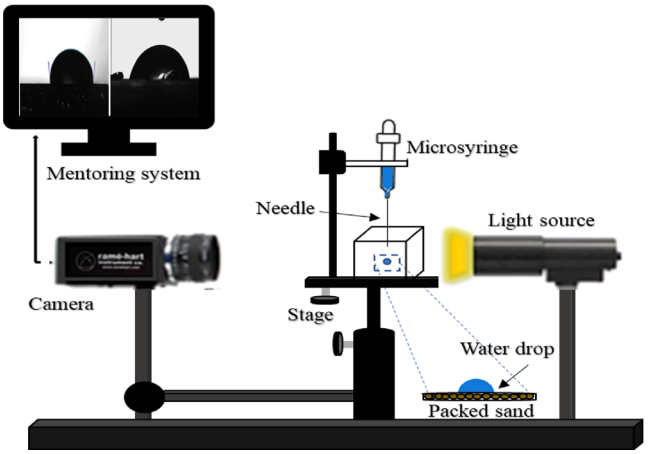

Figure 16. Contact angle measuring system.

first layer of polyurethane coating was applied and left to cure for one hour before spraying the second resin layer, which was lifted to cure for 24 h. The first layer's primary function is to act as a primer between the proppant surface and the second resin layer. Each coating layer was calibrated to be 1 wt % of the sand with a possible error of 5%. This fully cured (dried) polymeric thermoplastic coating can be constantly softened with no alteration in the chemical structure.[50] They can reassemble themselves regularly, and they can easily maintain their structure. The following are some of the most important benefits of thermoplastic polymers: (1) increased flexibility, superior impact resistance, and high fracture resilience, (2) high recycling and reuse potential, (3) excellent corrosion resistance, and (4) high moisture tolerance.[34] Tanguay et al.[51] provide further details on the chemical structures, physical properties, and mechanical properties of thermoplastic resin. Polyurethane was selected due to its quick curing at lower temperatures and the minimal impacts that it poses on the environment (i.e., not associated with green gas emission that requires advanced processing devices).[52] These factors potentially reduce the costs of developing coated proppants and allow the coating process to be executed on-site.

4.3. Assessment of Proppant Self-Aggregation (Flowback Control). *4.3.1. Quantitative Assessment.* Since there is no consistent evaluation method for assessing proppant self-aggregation properties, a gas loop system was designed and used to test the proppant self-aggregation property (flowback control), as shown in Figure 14. First, 5 g of different proppants (untreated sand, resin-coated sand, and resin-based nanocomposite-coated sand) was prepared and packed on a sleeve with an inner diameter of 10 mm and a length of 55 mm. Second, all the samples packed into sleeves were soaked into 35,000 ppm brine for 15 min. The brine composition is shown in Table 3.

Third, samples were collected and placed in the gas loop system. Finally, an air pressure of 496 kPa was induced in a sleeve through an inlet that contained packed sand surrounded by a sand covering screen. The sleeve outlet was connected to a container to collect the detached (flowed back) sand. The quantity of the detached sand particles collected indicates the proppant's self-aggregation ability and their potential to control the proppant flowback incident. The flowback percentage was determined using eq 3

$$\%\text{proppant flowback} = \frac{\text{Weight of collected detached proppant particles (g)}}{\text{Total weight of the proppant pack (g)}} \times 100 \quad (3)$$

This developed method's primary mechanism is that when the air dragging force is applied to proppant pack particles, the particles are progressively stripped from the proppant pack unless there is a strong linkage between those particles holding them together.

4.3.2. Qualitative Assessment. The qualitative assessment of proppant self-aggregation characteristics of resin-based nanocomposite-coated sand was conducted to observe the status of proppant particles scattered in water. First, the sample bottle was fed with 5 g of the untreated sand or resin-coated sand or resin-based nanocomposite-coated sand followed by 45 g of brine. The sample in the bottle was left for 10 min; then, the bottle was flipped upside down to observe the proppant ability of self-aggregation.

4.4. Proppant Crushing Resistance Testing. A proppant crushing resistance test was conducted at room temperature using a universal testing machine (UTM; model, Amsler HA100; manufacturer, ZwickRoell) that complied with the ISO 13503-2 proppant standard.[40] The date was recorded using a BiSS 2370SS series 32-bit controller. This test's primary goal was to determine the compaction and amount of fines produced by the proppant pack, both of which are essential factors affecting the conductivity. The crushing cell with a 30 mm diameter and a 70 mm length was packed with 5 g of the proppant, as shown in Figure 15. After loading the cell with the proppant grains, a vertical load was applied by the UTM machine at a constant displacement rate of 0.05 mm/min until it reached the targeted stress level. After attaining the targeted loading, the applied load was further maintained for 120 s. Thus, because the tested samples were loaded vertically, the constrained modulus was calculated to investigate the proppant pack compressibility. The constrained modulus refers to the ratio of stress to strain in the absence of lateral strain (no net lateral particle displacement) during compression in one dimension.[53] The crushed samples were sieved using seven different sizes of sieves to separate the generated fines and the sand grains.

4.5. Proppant Thermal Stability Measurement. Thermogravimetric analysis (TGA) was performed to investigate the thermal stability of polymeric polyurethane resin-coated sand (coated with 4 wt % polyurethane resin) and resin-based nanocomposite-coated sand (coated with 0.1 wt % MWCNTs followed by 4 wt % polyurethane resin) under elevated temperature conditions using loss on ignition (LOI). The samples were heated at a rate of 10 °C/min from 25 to 900 °C, and the LOI was monitored throughout.

4.6. Proppant Surface Wettability. Surface wettability is determined by the contact angle measurement when the liquid−vapor interface meets the solid−liquid interface. Materials are generally characterized as water-wet (hydrophilic) when $\theta < 90°$, oil-wet (hydrophobic) when $\theta > 90°$, or neutral (intermediate) wet when $\theta = 90°$.[54] Proppant scaling refers to the process in which minerals at the proppant surface react with other minerals and salts that precipitate to form scale deposition that reduce the permeability of the proppant pack.[25] To determine the ability of a resin-based nanocomposite coating to convert the coated sand surface from

https://doi.org/10.1021/acsomega.1c01639
ACS Omega 2021, 6, 20768−20778

hydrophilic to hydrophobic, the sessile drop method was used to determine the contact angle of a water droplet on the uncoated and coated sand substrates. A standard contact angle goniometer (model, ramé-hart 260; manufacturer, ramé-hart instrument co.; accuracy of contact angle, ±0.10°) was utilized for the measurement. The schematic of the system is provided in Figure 16.

AUTHOR INFORMATION

Corresponding Author

Ali Samer Muhsan − *Petroleum Engineering Department and Mechanical Engineering Department, Universiti Teknologi PETRONAS, 32610 Bandar Seri Iskandar, Perak, Malaysia*; Email: ali.samer@utp.edu.my, alisameer2007@gmail.com

Authors

Ali Aref Ali Alzanam − *Petroleum Engineering Department, Universiti Teknologi PETRONAS, 32610 Bandar Seri Iskandar, Perak, Malaysia*; orcid.org/0000-0002-3882-2902

Umair Ishtiaq − *Petroleum Engineering Department, Universiti Teknologi PETRONAS, 32610 Bandar Seri Iskandar, Perak, Malaysia*

Norani Muti Mohamed − *Centre of Innovative Nanostructures and Nanodevices (COINN), Universiti Teknologi PETRONAS, 32610 Seri Iskandar, Perak, Malaysia; Department of Fundamental and Applied Sciences, Universiti Teknologi PETRONAS, 32610 Seri Iskandar, Perak Darul Ridzuan, Malaysia*; orcid.org/0000-0003-0998-458X

Complete contact information is available at: https://pubs.acs.org/10.1021/acsomega.1c01639

Notes

The authors declare no competing financial interest.

ACKNOWLEDGMENTS

Authors express their thankful remarks to the Universiti Teknologi PETRONAS (UTP) Malaysia and Yayasan UTP for supporting the experimental part of this research under the YUTP research grant with cost center 015LC0-086.

REFERENCES

(1) Veatch, R. W.; Moschovidis, Z. A. An Overview of Recent Advances in HydrauLic Fracturing Technology. *International meeting on petroleum engineering*; Society of Petroleum Engineer: 1986, 421−454.

(2) Barati, R.; Liang, J.-T. A Review of Fracturing Fluid Systems Used for Hydraulic Fracturing of Oil and Gas Wells. *J. Appl. Polym. Sci.* **2014**, *131*, 1−11.

(3) Weaver, J.; Rickman, R.; Luo, H. Fracture-Conductivity Loss Caused by Geochemical Interactions between Man-Made Proppants and Formations. *SPE J.* **2010**, *15*, 116−124.

(4) Sanematsu, P.; Shen, Y.; Thompson, K.; Yu, T.; Wang, Y.; Chang, D. L.; Alramahi, B.; Takbiri-Borujeni, A.; Tyagi, M.; Willson, C. Image-Based Stokes Flow Modeling in Bulk Proppant Packs and Propped Fractures under High Loading Stresses. *J. Pet. Sci. Eng.* **2015**, *135*, 391−402.

(5) BAO, J.; LIU, H.; ZHANG, G.; JIN, J.; CHENG, W.; LIU, J. Fracture Propagation Laws in Staged Hydraulic Fracturing and Their Effects on Fracture Conductivities. *Pet. Explor. Dev.* **2017**, *44*, 306−314.

(6) LIU, N.; ZHANG, Z.; ZOU, Y.; MAMA, X.; ZHANG, Y. Propagation Law of Hydraulic Fractures during Multi-Staged Horizontal Well Fracturing in a Tight Reservoir. *Pet. Explor. Dev.* **2018**, *45*, 1129−1138.

(7) Li, Q.; Xing, H.; Liu, J.; Liu, X. A Review on Hydraulic Fracturing of Unconventional Reservoir. *Petroleum* **2015**, *1*, 8−15.

(8) Abdulelah, H.; Mahmood, S. M.; Al-Mutarreb, A. Effect of Anionic Surfactant on Wettability of Shale and Its Implication on Gas Adsorption/Desorption Behavior. *Energy Fuels* **2018**, *32*, 1423−1432.

(9) Abdulelah, H.; Negash, B. M.; Yekeen, N.; Al-Hajri, S.; Padmanabhan, E.; Al-Yaseri, A. Synergetic Effect of Surfactant Concentration, Salinity, and Pressure on Adsorbed Methane in Shale at Low Pressure: An Experimental and Modeling Study. *ACS Omega* **2020**, *5*, 20107−20121.

(10) Al-Muntasheri, G. A. A Critical Review of Hydraulic Fracturing Fluids over the Last Decade. *Soc. Pet. Eng. West. North Am. Rocky Mt. Jt. Conf. Exhib. 2014* **2014**, *2*, 621−644.

(11) Wen, Q.; Zhang, S.; Wang, L.; Liu, Y.; Li, X. The Effect of Proppant Embedment upon the Long-Term Conductivity of Fractures. *J. Pet. Sci. Eng.* **2007**, *55*, 221−227.

(12) Guo, T.; Zhang, S.; Wang, L.; Sui, W.; Wen, H. Optimization of Proppant Size for Frac Pack Completion Using a New Equipment. *J. Pet. Sci. Eng.* **2012**, *96-97*, 1−9.

(13) Khanna, A.; Kotousov, A.; Sobey, J.; Weller, P. Conductivity of Narrow Fractures Filled with a Proppant Monolayer. *J. Pet. Sci. Eng.* **2012**, *100*, 9−13.

(14) Bortolan Neto, L.; Khanna, A.; Kotousov, A. Conductivity and Performance of Hydraulic Fractures Partially Filled with Compressible Proppant Packs. *Int. J. Rock Mech. Min. Sci.* **2015**, *74*, 1−9.

(15) Fu, L.; Zhang, G.; Ge, J.; Liao, K.; Jiang, P.; Pei, H.; Li, X. Surface Modified Proppants Used for Porppant Flowback Control in Hydraulic Fracturing. *Colloids Surf., A* **2016**, *507*, 18−25.

(16) Liang, F.; Sayed, M.; Al-Muntasheri, G. A.; Chang, F. F.; Li, L. A Comprehensive Review on Proppant Technologies. *Petroleum* **2016**, *2*, 26−39.

(17) Pangilinan, K. D.; De Leon, A. C. C.; Advincula, R. C. Polymers for Proppants Used in Hydraulic Fracturing. *J. Pet. Sci. Eng.* **2016**, *145*, 154−160.

(18) Haque, M. H.; Saini, R. K.; Sayed, M. A. Nano-Composite Resin Coated Proppant for Hydraulic Fracturing. *Paper presented at the Offshore Technology Conference*; 2019, Houston, Texas, *2019-May*, DOI: 10.4043/29572-ms.

(19) Saldungaray, P.; Palisch, T.; Leasure, J. Can Proppants Do More than Hold the Fracture Open? *SPE Saudi Arabia Section Annual Technical Symposium and Exhibition*; Society of Petroleum Engineers: 2015, 21−23, DOI: 10.2118/177978-ms.

(20) Cooper, J. C.; Nguyen, P. D.; Magill, D. Field Application of a Water-Based Consolidation System for Remediation of Proppant Flowback. *SPE Asia Pacific Oil and Gas Conference and Exhibition*: Society of Petroleum: 2010, *3*, 1761−1777, DOI: 10.2118/134272-ms.

(21) Nguyen, P. D.; Weaver, J. D. Controlling Proppant Flowback in High-Temperature, High-Production Wells. *SPE European Formation Damage Conference*; Petroleum Engineers: 2003, DOI: 10.2523/82215-ms.

(22) Hu, J. H.; Zhao, J. Z.; Li, Y. M. A Proppant Mechanical Model in Postfrac Flowback Treatment. *J. Nat. Gas Sci. Eng.* **2014**, *20*, 23−26.

(23) Pope, C. D.; Wiles, T. J.; Pierce, B. R. Curable Resin-Coated Sand Controls Proppant Flowback. *SPE Production Operations Symposium*; Society of Petroleum Engineers: 1987, 265−272, DOI: 10.2118/16209-ms.

(24) Peard, N. S.; Macaluso, M. L.; Griffin, M. C.; Andress, R.; Callanan, M. J. Improved Fracturing Techniques Increase Productivity in the AWP (Olmos) Field. *SPE Production Operations Symposium*; Society of Petroleum Engineers: 1991, 141−148, DOI: 10.2118/21646-ms.

(25) Terracina, J. M.; Turner, J. M.; Collins, D. H.; Spillars, S. E. Proppant Selection and Its Effect on the Results of Fracturing Treatments Performed in Shale Formations. *SPE Annual Technical*

Conference and Exhibitio; OnePetro: 2010, *6*, 5092−5108, DOI: 10.2118/135502-ms.
(26) Vo, L. K.; Nguyen, P. D.; Liang, F.; Parton, C. Enhancing Proppant Pack Conductivity With Consolidation and Agglomeration Performance: A Laboratory Study. *SPE International Symposium and Exhibition on Formation Damage Control*; Society of Petroleum Engineers: 2014, DOI: 10.2118/168188-ms.
(27) Lu, W.; O'Neil, B.; Zhang, K.; Wang, C.; Quintero, H. *Enhancing Proppant Flowback Control Through Surface Treatment of Proppant*; *International Petroleum Technology Conference*; International Petroleum Technology Conference: 2016, DOI: 10.2523/18796-ms.
(28) Burukhin, A.; Kalinin, S.; Abbott, J.; Bulova, M.; Wu, Y.; Crandall, M.; Kadoma, I.; Begich, M.; Papp, S. Novel Interconnected Bonded Structure Enhances Proppant Flowback Control. *SPE International Symposium and Exhibition on Formation Damage Control*; Society of Petroleum Engineers 2012, *2* (February), 1075−1091, DOI: 10.2118/151861-ms.
(29) Nguyen, P. D.; Weaver, J. D.; Parker, M. A.; King, D. G.; Gillstrom, R. L.; Batenburg, D. W. V. Proppant Flowback Control Additives. *SPE Annual Technical Conference and Exhibition*; Society of Petroleum Engineers: 1996, 119−131, DOI: 10.2523/36689-ms.
(30) McLennan, J.; Walton, I.; Moore, J.; Brinton, D.; Lund, J. Proppant Backflow: Mechanical and Flow Considerations. *Geothermics* **2015**, *57*, 224−237.
(31) Gidley, J. L.; Penny, G. S.; McDaniel, R. R. Effect of Proppant Failure and Fines Migration on Conductivity of Propped Fractures. *SPE Prod. Facil.* **1995**, *10*, 20−25.
(32) Ellis, P. D.; Surles, B. W. Chemically Inert Resin Coated Proppant System For Control of Proppant Flowback In Hydraulically Fractured Wells. U.S. Patent 5,604,184,*Geothermics* **1985**, *14* (4), 595−599.
(33) Nguyen, P. D.; Dewprashad, B. T.; Weaver, J. D. SPE 50002 A New Approach for Enhancing Fracture Conductivity. SPE Asia Pacific Oil and Gas Conference and Exhibition; Society of Petroleum Engineers: 1998, 109−122.
(34) Zoveidavianpoor, M.; Gharibi, A. Application of Polymers for Coating of Proppant in Hydraulic Fracturing of Subterraneous Formations: A Comprehensive Review. *J. Nat. Gas Sci. Eng.* **2015**, *24*, 197−209.
(35) Duenckel, R. J.; Barree, R. D.; Llc, A.; Drylie, S.; Connell, L. G. O.; Abney, K. L. Proppants- What 30 Years of Study has Taught Us. *SPE Annual Technical Conference and Exhibition*; Society of Petroleum Engineers: 2017.
(36) Gomez, V.; Alexander, S.; Barron, A. R. Proppant Immobilization Facilitated by Carbon Nanotube Mediated Microwave Treatment of Polymer-Proppant Structures. *Colloids Surf., A* **2017**, *513*, 297.
(37) Alexander, S.; Dunnill, C. W.; Barron, A. R. Assembly of Porous Hierarchical Copolymers/Resin Proppants: New Approaches to Smart Proppant Immobilization via Molecular Anchors. *J. Colloid Interface Sci.* **2016**, *466*, 275−283.
(38) Wang, M.; Zhang, J.; Zhou, S.; Yang, Z.; Zhang, X. Glass Transition Behaviour of Thin Polymer Films Coated on the 3D Networks of Porous CNT Sponges. *Phys. Chem. Chem. Phys.* **2020**, 21297.
(39) Omidvar, M.; Iskander, M.; Bless, S. Stress-Strain Behavior of Sand at High Strain Rates. *Int. J. Impact Eng.* **2012**, *49*, 192−213.
(40) ISO 8894-2. International Standard International Standard. *61010−1 © Iec2001* **2006**, *2006*, 13.
(41) Habibi, A.; Ahmadi, M.; Pourafshary, P.; Ayatollahi, S. Reducing Fines Migration by Use of Nanofluids Injection-an Experimental Study. *JPT, J. Pet. Technol.* **2011**, *63*, 106−110.
(42) Huang, T.; Crews, J. B.; Willingham, J. R. Nanoparticles for Formation Fines Fixation and Improving Performance Surfactant Structure Fluids. *Int. Pet. Technol. Conf. IPTC 2008* **2008**, *3*, 1558−1567.
(43) Qian, T.; Muhsan, A. S.; Htwe, L.; Mohamed, N.; Hussein, O. Urethane Based Nanocomposite Coated Proppants for Improved Crush Resistance during Hydraulic Fracturing. In *IOP Conference Series: Materials Science and Engineering*; IOP Publishing: 2020, DOI: 10.1088/1757-899X/863/1/012013.
(44) Kumar, A.; Sharma, K.; Dixit, A. R. A Review on the Mechanical Properties of Polymer Composites Reinforced by Carbon Nanotubes and Graphene. *Carbon Lett.* **2021**, *31*, 149−165.
(45) Król, P.; Król, B. Surface Free Energy of Polyurethane Coatings with Improved Hydrophobicity. *Colloid Polym. Sci.* **2012**, *290*, 879−893.
(46) Sheet, T. D. *RPM Neutral Wettability Relative Permeability Modification Technology*https://carboceramics.com/products/proppant-technologies/flow-enhancing-proppant/rpm-product-detail (Accessed on January 24, 2021).
(47) Gomez, V.; Irusta, S.; Lawal, O. B.; Adams, W.; Hauge, R. H.; Dunnill, C. W.; Barron, A. R. Enhanced Purification of Carbon Nanotubes by Microwave and Chlorine Cleaning Procedures. *RSC Adv.* **2016**, *6*, 11895−11902.
(48) He, X. Q.; Kitipornchai, S.; Wang, C. M.; Liew, K. M. Modeling of van Der Waals Force for Infinitesimal Deformation of Multi-Walled Carbon Nanotubes Treated as Cylindrical Shells. *Int. J. Solids Struct.* **2005**, *42*, 6032−6047.
(49) Mao, J.; Liu, M.; Deng, Z.; Deng, C.; Deng, C.; Zhou, K. Influence of Spray Angle on Distribution of WC-Co-Cr Coating Produced by HVOF Spraying. *Rare Met. Mater. Eng.* **2017**, *46*, 3583−3588.
(50) Sinclair, A.; Akbar, S.; Okell, R. Process For Incremental Coating Of Proppants For Hydraulic Fracturing And Proppants Produced Therefrom U.S. Patent US 8,852,682 B2 ,Oct. 7, 2014.
(51) Tanguay, M.; Kerobo, O.; Roh, Y.; Gross, F. A proppant U.S. Patent. WO 2014/093229, June,19, 2014.
(52) Robert, M.; Avis, L. Coated And Cured Proppants U.S. Patent US 8,993,489 B2, Mar. 31, 2015.
(53) Gemperline, M.; Gemperline, E.; Gemperline, C. *LARGE SCALE CONSTRAINED MODULUS TEST*. https://plasticpipe.org/pdf/ms-study-report.pdf, 2010 (Accessed on April 15, 2021).
(54) Maghzi, A.; Mohammadi, S.; Ghazanfari, M. H.; Kharrat, R.; Masihi, M. Monitoring Wettability Alteration by Silica Nanoparticles during Water Flooding to Heavy Oils in Five-Spot Systems: A Pore-Level Investigation. *Exp. Therm. Fluid Sci.* **2012**, *40*, 168−176.

https://doi.org/10.1021/acsomega.1c01639
ACS Omega 2021, 6, 20768−20778